ECOHYDROLOGY
Ecohydrol. **7**, 139–149 (2014)
Published online 21 November 2012 in Wiley Online Library
(wileyonlinelibrary.com) DOI: 10.1002/eco.1341

Estimation of evapotranspiration over the terrestrial ecosystems in China

Xianglan Li,[1,2] Shunlin Liang,[1,2,3]* Wenping Yuan,[1,2]* Guirui Yu,[4] Xiao Cheng,[1,2] Yang Chen,[1,2] Tianbao Zhao,[5] Jinming Feng,[2,5] Zhuguo Ma,[5] Mingguo Ma,[6] Shaomin Liu,[7] Jiquan Chen,[8] Changliang Shao,[9] Shenggong Li,[10] Xudong Zhang,[11] Zhiqiang Zhang,[12] Ge Sun,[13] Shiping Chen,[9] Takeshi Ohta,[14] Andrej Varlagin,[15] Akira Miyata,[16] Kentaro Takagi,[17] Nobuko Saiqusa[18] and Tomomichi Kato[19]

[1] *State Key Laboratory of Remote Sensing Science, Beijing Normal University, Institute of Remote Sensing Applications of the Chinese Academy of Sciences, Beijing 100875, China*
[2] *College of Global Change and Earth System Science, Beijing Normal University, Beijing 100875, China*
[3] *Department of Geography, University of Maryland, College Park, MD 20742, USA*
[4] *Key Laboratory of Ecosystem Network Observation and Modeling, Synthesis Research Center of the Chinese Ecosystem Research Network, Institute of Geographic Sciences and Natural Resources Research, Chinese Academy of Sciences, Beijing 100101, China*
[5] *Key Laboratory of Regional Climate-Environment Research for Temperate East Asia, Institute of Atmospheric Physics, Chinese Academy of Sciences, Beijing 100029, China*
[6] *Cold and Arid Regions Environmental and Engineering Research Institute, Chinese Academy of Sciences, Lanzhou, Gansu 730000, China*
[7] *State Key Laboratory of Remote Sensing Science, School of Geography, Beijing Normal University, Beijing 100875, China*
[8] *Department of Environmental Sciences, University of Toledo, Toledo, OH 43606, USA*
[9] *State Key Laboratory of Vegetation and Environmental Change, Institute of Botany, Chinese Academy of Sciences, Beijing 100093, China*
[10] *Institute of Geographic Sciences and Natural Resources Research, Chinese Academy of Sciences, Beijing 100101, China*
[11] *Institute of Forestry Research, Chinese Academy of Forestry, Beijing 100091, China*
[12] *College of Soil and Water Conservation, Beijing Forestry University, Beijing 100083, China*
[13] *Eastern Forest Environmental Threat Assessment Center, Southern Research Station, Raleigh, NC 27606, USA*
[14] *Graduate School of Bioagricultural Sciences, Nagoya University, Nagoya 464-8601, Japan*
[15] *A.N. Severtsov Institute of Ecology and Evolution Russian Academy of Sciences, Moscow 119071, Russia*
[16] *National Institute for Agro-Environmental Sciences, Tsukuba 305-8604, Japan*
[17] *Teshio Experimental Forest, Field Science Center for Northern Biosphere, Hokkaido University, Teshio 098-2943, Japan*
[18] *Center for Global Environmental Research National Institute for Environmental Studies, Tsukuba, Ibaraki 305-8506, Japan*
[19] *National Institute for Environmental Studies, Tsukuba, Ibaraki 305-8569, Japan*

ABSTRACT

Quantifying regional evapotranspiration (ET) and environmental constraints are particularly important for understanding water and carbon cycles of terrestrial ecosystems. However, a large uncertainty in the regional estimation of ET still remains for the terrestrial ecosystems in China. This study used ET measurements of 34 eddy covariance sites within China and adjacent regions to examine the performance of the revised Remote Sensing-Penman Monteith (RS-PM) model over various ecosystem types including forests, grasslands, wetlands and croplands. No significant systematic error was found in the revised RS-PM model predictions, which explained 61% of the ET variations at all of the validation sites. Regional patterns of ET at a spatial resolution of 10×10 km were quantified using a meteorology dataset from 753 meteorological stations, Modern Era Retrospective-analysis for Research and Applications (MERRA) reanalysis products and satellite data such as the Advanced Very High Resolution Radiometer (AVHRR) leaf area index. ET decreased from the southeast of China toward the northwest. Relatively high ET values were found in the southern China such as Yunnan, Hainan, Fujian and Guangdong Provinces, whereas low ET values occurred in northwestern China such as in the Xinjiang autonomous region. On average, the annual ET presented an increasing trend during the 1982–2009, with relatively low ET in 1985, 1993, 1997, 2000 and 2009. We found that the mean annual ET was higher than world average, ranging spatially between 484 and 521 mm yr^{-1}, with a mean value of 500 mm yr^{-1}, which accounted for approximately 5·6–8·3% of the world's total land-surface ET. Copyright © 2012 John Wiley & Sons, Ltd.

KEY WORDS evapotranspiration; Remote Sensing-Penman Monteith model; AVHRR; MERRA; eddy covariance

Received 24 April 2012; Revised 17 September 2012; Accepted 28 September 2012

INTRODUCTION

Evapotranspiration (ET) over land, the sum of water lost to the atmosphere from the soil surface through evaporation and from plant tissues via transpiration, is a key component of the hydrological, energy and carbon cycles (Dirmeyer, 1994; Pielke *et al.*, 1998; Cleugh *et al.*, 2007; Mu *et al.*, 2007a, b; Jung *et al.*, 2010; Sun *et al.*, 2011). Approximately 60–80%

*Correspondence to: Shunlin Liang, Department of Geography, University of Maryland, College Park, MD 20742, USA; Wenping Yuan, College of Global Change and Earth System Science, Beijing Normal University, Beijing 100875, China. E-mail: sliang@umd.edu; wenpingyuancn@yahoo.com

of the precipitation on the earth's surface returns to the atmosphere as ET that becomes the source of future precipitation in the regional and global water cycles (Baumgartner and Reichel, 1975; Tateishi, 1996; Oki and Kanae, 2006). Therefore, changes in ET have a great impact on the global hydrologic cycle and energy budget (Xu and Singh, 2005; Gao *et al.*, 2007). Quantifying temporal and spatial patterns of ET is critical for understanding the interactions between land surfaces and the atmosphere, improving water and land resource management (Meyer, 1999; Raupach, 2001), detecting and assessing droughts (McVicar and Jupp, 1998) and performing regional hydrological applications (Kustas and Norman, 1996; Keane *et al.*, 2002).

A number of ecosystem process models are available for quantifying spatio-temporal variations of ET at large scales, such as the Surface Energy Balance System (Kalma and Jupp, 1990; Bastiaanssen *et al.*, 1998; Su, 2002), the Penman–Monteith algorithm (Penman, 1948; Monteith, 1964; Cleugh *et al.*, 2007; Mu *et al.*, 2007a, b; Yuan *et al.*, 2007, 2010; Vinukollu *et al.*, 2011), the Priestley–Taylor-based approach (Priestley and Taylor, 1972; Fisher *et al.*, 2008) and the water-centric monthly scale simulation model (Sun *et al.*, 2011). However, large uncertainties in ET estimation still remain (Li *et al.*, 2009). For instance, a comparison of 15 model simulations from the Global Soil Wetness Project-2 suggested that the lowest estimation of global mean ET, with a value of 272 mm yr^{-1}, was approximately 38% smaller than the maximum estimation of 442 mm yr^{-1} (Dirmeyer *et al.*, 2006).

Most of the regional ET studies have focused on reference ET (Chen *et al.*, 2005; Gong *et al.*, 2006; Thomas, 2008), potential ET (Thomas, 2000; Gao *et al.*, 2006), pan ET (Liu *et al.*, 2004; Cong *et al.*, 2008) and actual ET at river basin and regional scales (Chen *et al.*, 2003, 2006; Zeng *et al.*, 2010a, b; Zhang *et al.*, 2010). Sun *et al.* (2004) investigated the spatial distribution of ET in the Changbaishan Natural Reserve of China using Landsat ETM + data and the boreal ecosystem productivity simulator model. They found that annual ET decreased greatly with altitude, from greater than 600 mm at the foot of the mountain to approximately 200 mm at the top of the mountain, and ET was the highest for broadleaf forests and the lowest for urban and built-up areas. Regional daily ET rates in the Sanjiang Plain were estimated based on the surface energy balance algorithm for land (Du *et al.*, 2010). ET rates of dry crops (428 mm) and paddy fields (480 mm) were lower than wetlands (554 mm) and forests (659 mm). According to the Surface Energy Balance System model, the annual ET in 2005 over the Yellow River Delta wetlands was 947 mm (Jia *et al.*, 2009). Thomas (2000) analysed ET using the PM method based on 65 stations in China for the time series 1954–1993. The analysis indicated that northeast and southwest China experienced a moderate ET increase, whereas northwest and southeast China were associated with a decreasing trend. However, because of the limited access to climate data and/or different focuses, the existing works only focus on limited parts of China or use a small number of selected stations and eddy covariance (EC) sites over China. Also, different ecosystem models gave inconsistent ET values in the magnitude and spatial-temporal distribution at a large scale (Thomas, 2000; Xu *et al.*, 2006a, b).

The Remote Sensing-Penman Monteith ET model was developed based on energy balance and mass transfer and considers aerodynamic resistance and surface resistance. The model has been successfully used to calculate actual ET from different land covers and varying climate conditions (Monteith, 1965; Cleugh *et al.*, 2007; Mu *et al.*, 2007a, b, 2009; Yuan *et al.*, 2007, 2010). Worldwide EC measurements offer the best opportunity for calibrating or validating ecosystem models for regional estimate of water fluxes (Xiao *et al.*, 2011; Sun *et al.*, 2011). However, because of the scarcity of observations, the revised RS-PM model has not been validated for China. The objectives of this study were to (1) evaluate the performance of the revised RS-PM model over various terrestrial ecosystems within China and adjacent regions based on the measurements from 34 EC sites and (2) quantify the spatial and temporal patterns of ET among different vegetation types in China during 1982–2009 period.

METHODS AND MATERIALS

The revised RS-PM model

The RS-PM model was originally proposed by Cleugh *et al.* (2007), who reported a methodology that estimates 8-day ET at a 1-km spatial resolution using gridded meteorological fields and the PM equation (Monteith, 1965). Mu *et al.* (2007a, b) revised the surface conductance model of Cleugh *et al.* (2007) to produce a global ET algorithm by accounting for stomatal responses to temperature and an atmospheric humidity deficit and by introducing a separate soil evaporation term that was no explicitly considered by Cleugh *et al.* (2007). Previous studies, however, have demonstrated that high air temperature significantly decreases leaf stomatal conductance by closing stomata and causing structural defects (Schreiber *et al.*, 2001). Therefore, we further revised the equations dealing with temperature constraint by accounting for stomatal conductance and energy allocation between the vegetation canopy and soil surface, and we used the Beer–Lambert law to exponentially partition the net radiation between the canopy and the soil surface (Ruimy *et al.*, 1999). In the latest study, we calibrated three parameters of the revised RS-PM model: VPD_{close}, the total aerodynamic conductance to vapour transport, C_{tot}, the sum of soil surface conductance and the aerodynamic conductance for vapour transport and C_l, the mean potential stomatal conductance. We used the observed ET from all of the eddy flux towers to set constant parameters for all of the vegetation types, with the results of 0·008 m s^{-1} for C_{tot}, 0·003 m s^{-1} for C_l and 2·79 kPa for VPD_{close} (Yuan *et al.*, 2010). The revised RS-PM model was calibrated and validated with the AmeriFLUX and EuroFLUX sites that are dominated by six major terrestrial biomes, explaining 82% and 68% of the observed variations of ET for all of the calibration and validation sites, respectively (Yuan *et al.*, 2010).

Data at EC sites

Eighteen EC sites from Coordinated Observations and Integrated Research over Arid and Semi-arid China were included in this study to validate the revised RS-PM model, covering multiple ecosystem types in China such as grasslands, croplands and wetlands (Table I). To validate the RS-PM model on forest ecosystems, three ChinaFlux sites including Changbaishan, Dinghushan, and Qianyanzhou were used. Also, some forest EC sites in China and adjacent regions from AsiaFlux and FluxNet networks were included because similar forest type and climate were found between China and the adjacent regions such as Russia and Japan. For each tower, we obtained the ET estimates using the revised RS-PM algorithm and compared them with the observed ET. We aggregated the half-hourly data into daily data, and the daily values were indicated as missing when more than 20% of the data were missing for a given day; otherwise, the daily values were calculated by multiplying the averaged hourly rate by 24 h.

The leaf area index (LAI) for the sites were determined from moderate resolution imaging spectroradiometer (MODIS) data. MODIS ASCII (American Standard Code for Information Interchange) subset data used in this study were generated from MODIS Collection 5 data that was downloaded directly from the Oak Ridge National Laboratory Distributed Active Center website. The 8-day MODIS LAI (MOD15A2) data at 1-km spatial resolution were the basis for model verification in the flux sites. Only the LAI values of the pixel containing the tower were used. Quality control flags, which signal cloud contamination in each pixel, were examined to screen and reject poor quality LAI data.

Regional data

For regional estimates of ET, we used input datasets for air temperature (Ta), relative humidity (RH) and precipitation (Prec) obtained from 753 stations in China by thin plate smoothing spline interpolation method. We also used net radiation (Rn) from the Modern Era Retrospective-analysis for Research and Applications (MERRA) dataset and resample into the spatial resolution of 10×10 km (Global Modeling and Assimilation Office, 2004). Detailed information on the MERRA dataset is available at the website http://gmao.gsfc.nasa.gov/research/merra.

We chose 1982–2009 as the study period for estimating regional ET based on the satellite-observed vegetation attributes and daily surface meteorology inputs. To produce a continuous and consistent time series LAI from 1982 to 2009, we combined AVHRR LAI and MODIS LAI, which were acquired from different sensors. The method of analyzing

Table I. Name, location, vegetation types and available years of the study sites used for the revised RS-PM model validation.

Site name	Latitude, longitude	Vegetation type	Available years
CN-Du	42·05°N, 116·67°W	Cropland	2005–2006
Miyun	40·63°N, 117·32°W	Cropland	2008–2009
MSE	36·05°N, 140·03°W	Cropland	2001–2004
Yuzhong	35·95°N, 104·13°W	Cropland	2008–2009
Guantao	36·52°N, 105·13°W	Cropland/maize	2009
Jinzhou	41·18°N, 121·21°W	Cropland/maize	2008–2009
Linze	39·35°N, 100·13°W	Cropland/maize	2008–2009
TongyuCrop	44·57°N, 122·88°W	Cropland/maize	2009
Yingke	38·86°N, 100·41°W	Cropland/maize	2008–2009
CBS	42·40°N, 127·09°W	Forest	2003–2008
CN-Anh	30·48°N, 116·98°W	Forest	2005–2006
CN-Bed	39·53°N, 116·25°W	Forest	2005–2006
DHS	23·17°N, 112·53°W	Forest	2002–2008
JP-Tef	45·06°N, 142·11°W	Forest	2002–2006
JP-Tom	42·74°N, 141·52°W	Forest	2001–2004
MBF	44·38°N, 142·32°W	Forest	2004–2006
QYZ	26·74°N, 115·07°W	Forest	2002–2008
RU-Fyo	56·46°N, 32·92°W	Forest	2000–2006
RU-Zot	60·80°N, 89·35°W	Forest	2002–2005
SKT	48·35°N, 108·65°W	Forest	2003–2007
TKY	36·15°N, 137·42°W	Forest	1999–2007
Arou	38·04°N, 100·46°W	Grassland	2008–2009
Changwu	35·20°N, 107·67°W	Grassland	2008–2009
CN-HaM	37·37°N, 101·18°W	Grassland	2002–2004
Dongsu	44·09°N, 113·57°W	Grassland	2008–2009
DuolunFenced	42·04°N, 116·29°W	Grassland	2009–2010
DuolunGrazed	42·05°N, 116·28°W	Grassland	2009–2010
KBU	47·21°N, 108·74°W	Grassland	2003–2009
Qingyang	35·59°N, 107·54°W	Grassland	2009
SiziwangFenced	41·23°N, 111·57°W	Grassland	2010
SiziwangGrazed	41·28°N, 111·68°W	Grassland	2010
TongyuGrass	44·57°N, 122·88°W	Grassland	2008–2009
Zhangye	39·09°N, 100·30°W	Grassland	2008
Maqu	34·0°N, 102·0°W	Alpine wetland	2009

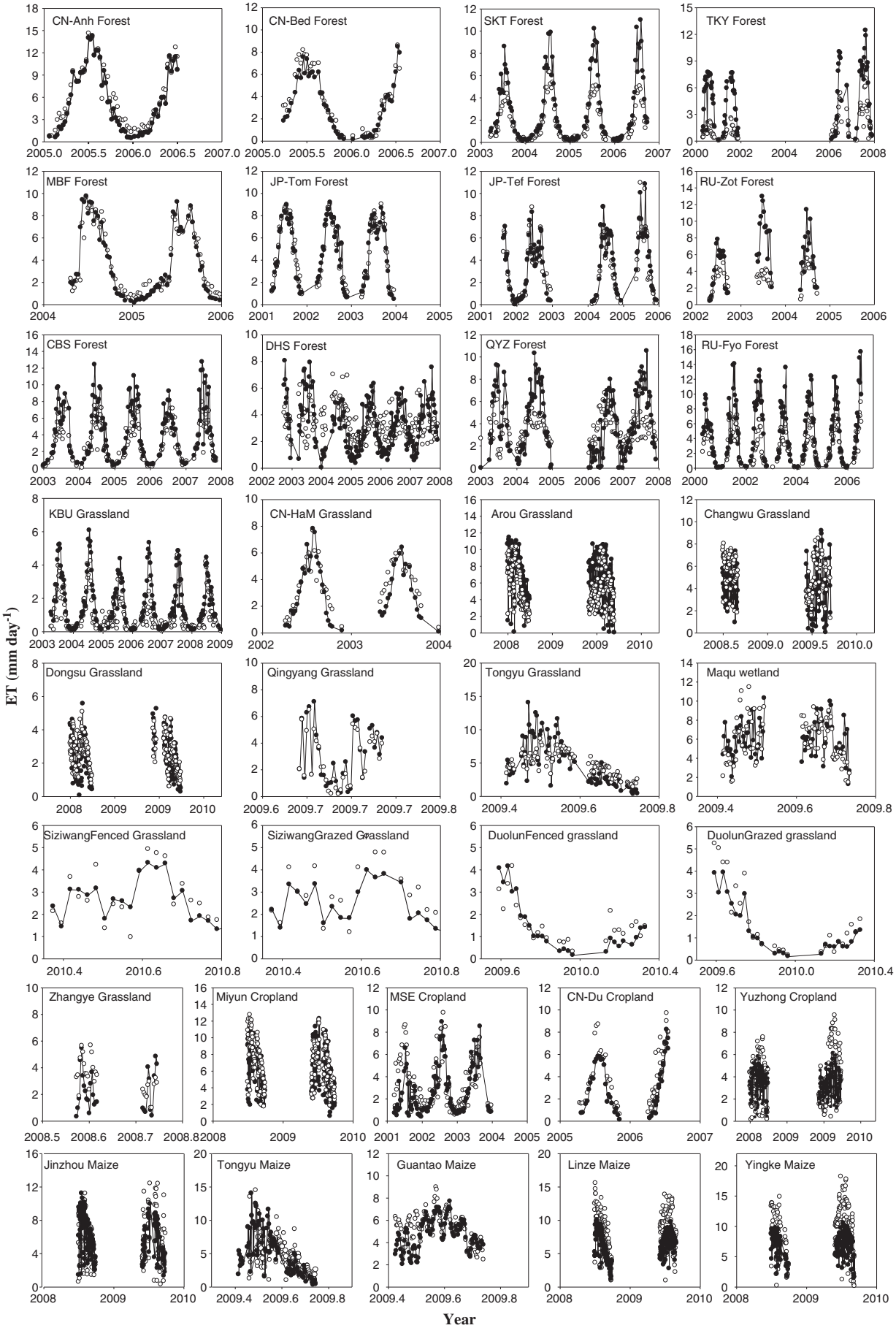

Figure 1. Variation in the 8-day mean value of the predicted ET and the observed ET at the model validation sites. The black solid lines represent the predicted ET, and the open circle dots represent the observed ET.

these two sets of data was described in Yuan *et al.* (2012). In brief, the AVHRR LAI products from 1982 to 2000 are based on a monthly maximum value compositing of AVHRR spectral reflectance data to mitigate cloud cover, smoke and other atmospheric aerosol contamination effects (http://cybele.bu.edu; Myneni *et al.*, 1997). The 8-day MODIS LAI (MOD15A2) data were used in this study from 2000 to 2009. Linear regression method was used to combine the two LAI series into a single and continuous record (Zhang *et al.*, 2008). Quality control flags were examined to screen and reject LAI data with insufficient quality. We temporally filled the missing or unreliable LAI at each 1-km MODIS pixel based on their corresponding quality assessment data fields as proposed by Zhao *et al.* (2005). If the first (or last) 8-day LAI data are unreliable or missing, they will be replaced by the closest reliable 8-day values.

For each tower and each algorithm, we estimated ET using two different sets of meteorological data: (1) integrated meteorological data derived from the half-hour observations at the flux tower sites and (2) the MERRA meteorological data at a 10×10-km resolution. For each tower, we calculated the ET for the vegetated 10×10-km pixels surrounding each site with the pre-processed AVHRR data, and we averaged the ET across all pixels. These averages were then compared with the tower ET observations.

Statistical analysis

Three metrics were used to evaluate the performance of the revised RS-PM model in this study:

1. The coefficient of determination, R^2, which represents how much variation in the observations was explained by the models.
2. Absolute predictive error (PE), which quantifies the difference between the simulated and observed values:

$$PE = \bar{S} - \bar{O} \quad (1)$$

where S and O are mean simulated and mean observed values, respectively.

3. Relative predictive error (RPE), computed as follows:

$$RPE = \frac{\bar{S} - \bar{O}}{\bar{O}} \times 100\% \quad (2)$$

Moreover, we used the standard deviation (std) of the annual ET to characterize the absolute interannual variability, and the coefficient of variation (CV, the ratio of std and the mean value of annual ET) was used to characterize the relative interannual variability.

RESULTS AND DISCUSSION

Model performance

Over the various ecosystem types, such as forests, croplands, grasslands and wetlands, the revised RS-PM model successfully predicted the magnitudes and seasonal variations of ET derived from the observed environmental variables (i.e. Ta, LAI, RH and Rn) (Figure 1). The predicted and observed ET from the EC measurement time series at the validation sites demonstrated distinct seasonal cycles and matched well. At most sites, the ET values were high during the plant growing season and almost near zero in the winter because of the low temperatures and plant growth limitation. Collectively, the revised RS-PM model successfully predicted the magnitudes and seasonal variations of the observed ET and explained approximately 61% of the variation of the 8-day ET at the 34 validation sites (Figure 2). Individually, the coefficients of determination (R^2) were all statistically significant at $p < 0{\cdot}05$ and varied from 0·32 at the Zhangye grassland site to 0·97 at the MBF forest site (Table II). This result showed that the RS-PM model was robust and reliable across most of the biomes and geographic regions in China. However, large differences between the predicted and observed ET still existed in a few sites. For example, the predicted ET values were higher than the observed ET at Changwu, RU-Fyo, SKT, TKY and KBU, with the RPE values ranging from 32% to 78% (Table II). At the other EC sites, the revised RS-PM model was a good predictor when RPE values were less than 20%.

Several potential sources of uncertainty in the ET calculations were linked to the corresponding uncertainties in the satellite data, meteorological reanalysis data and EC flux measurements. The revised RS-PM model used MODIS LAI products at EC sites and AVHRR LAI products for regional estimation, which were downloaded directly from the web site. No attempt was made to improve the quality of the LAI data. Therefore, any noise or errors in the satellite data were transferred to the ET simulations. Also, we used the global 8-day MODIS LAI at a 1-km resolution to derive the LAI record at each EC site. The tower measurement footprints are normally much smaller than the resolution of the overlying grid cell. The satellite-derived LAI may not adequately capture sub-grid scale vegetation signals at these sites, especially in areas of complex topography or heterogeneous land cover; thus, the model error for some tower sites may be attributed to inaccurate LAI representations of the tower footprint conditions.

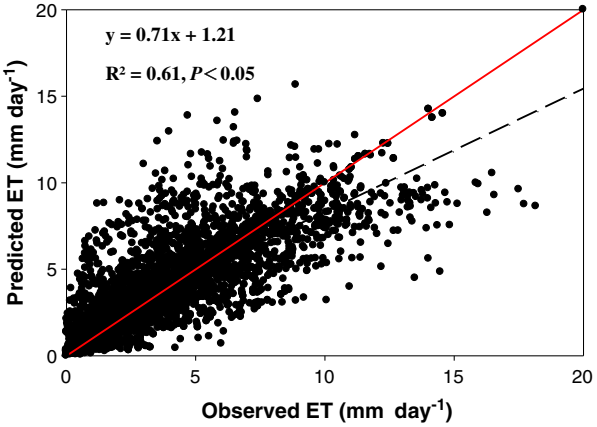

Figure 2. Comparison of the ET observations from the EC flux tower sites and predicted by the revised RS-PM model.

Table II. Predictions of the revised RS-PM model at 34 EC validation sites.

Site name	Revised RS-PM model				
	ET_{obs}	ET_{est}	PE	RPE	R^2
CN-Du	3·81	3·58	−0·23	−0·06	0·86
Miyun	5·98	6·85	0·87	0·15	0·82
MSE	3·34	2·85	−0·50	−0·15	0·61
Yuzhong	3·59	3·47	−0·12	−0·03	0·47
Guantao	5·29	4·66	−0·63	−0·12	0·37
Jinzhou	5·63	5·84	0·22	0·04	0·54
Linze	8·57	6·23	−2·34	−0·27	0·53
TongyuCrop	4·85	4·46	−0·39	−0·08	0·41
Yingke	5·12	4·26	−0·66	−0·18	0·73
CBS	3·42	2·91	−0·51	−0·15	0·74
CN-Anh	4·76	4·18	−0·58	−0·12	0·96
CN-Bed	4·69	3·93	−0·76	−0·16	0·95
DHS	4·21	4·23	0·02	0·01	0·52
JP-Tef	3·41	4·11	0·7	0·20	0·93
JP-Tom	4·52	4·31	−0·21	−0·05	0·95
MBF	2·20	2·55	0·35	0·16	0·97
QYZ	4·89	3·90	−1·00	−0·20	0·81
RU-Fyo	3·20	5·31	2·11	0·66	0·71
RU-Zot	3·77	3·04	−0·73	−0·19	0·41
SKT	2·04	2·93	0·89	0·44	0·95
TKY	1·92	4·27	3·34	0·78	0·60
Arou	6·43	5·3	−1·14	−0·18	0·76
Changwu	3·91	5·16	1·25	0·32	0·44
CN-HaM	3·46	3·6	0·15	0·04	0·86
Dongsu	2·19	2·52	0·33	0·15	0·39
DuolunFenced	1·61	1·43	−0·18	−0·11	0·69
DuolunGrazed	1·84	1·4	−0·44	−0·24	0·92
KBU	1·18	1·85	0·68	0·57	0·73
Qingyang	3·10	2·77	−0·33	−0·11	0·92
SiziwangFenced	2·58	2·49	−0·09	−0·04	0·81
SiziwangGrazed	2·81	2·3	−0·50	−0·18	0·88
TongyuGrass	4·75	4·74	−0·01	0·01	0·69
Zhangye	2·24	3·19	0·96	0·23	0·32
Maqu	5·90	5·81	−0·09	−0·02	0·56

CBS, Changbaishan; DHS, Dinghushan; KBU, Kherlenbayan Ulaan; MSE, Mase paddy flux site; MBF, Moshiri Birch Forest; QYZ, Qianyanzhou; SKT, Southern Khentei Taiga; TKY, Takayama Deciduous. ET_{obs} is ET that was observed at EC sites (mm day^{-1}). ET_{est} is ET that was predicted by the revised RS-PM model (mm day^{-1}). PE is the absolute predictive error. RPE is the relative predictive error. R^2 is the coefficient of determination.

The accuracy of the regional or global estimates of ET was also highly dependent on the meteorology datasets. We used the MERRA dataset at a resolution of 10×10 km to drive the revised RS-PM model. However, the accuracy of the existing meteorological reanalysis datasets showed marked differences both spatially and temporally. The model driven by the tower-specific meteorology data explained 64% of the annual mean ET variations across the 34 validation sites, and it produced no systematic errors in the model predictions (Figure 3a). In contrast, using the MERRA dataset significantly decreased the model performance, and the model explained 57% of the ET variations (Figure 3b).

Aside from systematic errors associated with EC methods and remote sensing technique, possible bias in our model and data included energy enclose problems that might cause ET estimation errors at EC sites. The general phenomena of incomplete energy balance closure at EC sites causes underestimation of sensible heat and latent heat flux and then underestimated ET about 20% (Wilson *et al.*, 2002). And there was about 10% absolute uncertainty in energy balance measurement caused by incomplete closure problem for EC method (Twine *et al.*, 2000).

Spatial patterns of ET

The revised RS-PM model was implemented over the terrestrial ecosystems of China from 1982 to 2009 at a resolution of 10×10 km. There was evidence of strong regional variations and latitudinal gradients of ET, with ET decreasing from the southeast to the northwest (Figure 4a). We estimated a mean annual ET value of 500 mm yr^{-1} from 1982 to 2009 across the various ecosystem types. The annual ET was generally low in the arid/semiarid regions of northwest China and the northeast region, whereas relatively high annual ET values were located in the south of China.

From the standpoint of national territory, relatively high annual ET values were found in Hainan, Taiwan, Yunnan, Guangdong, Fujian and Guizhou provinces, with ET

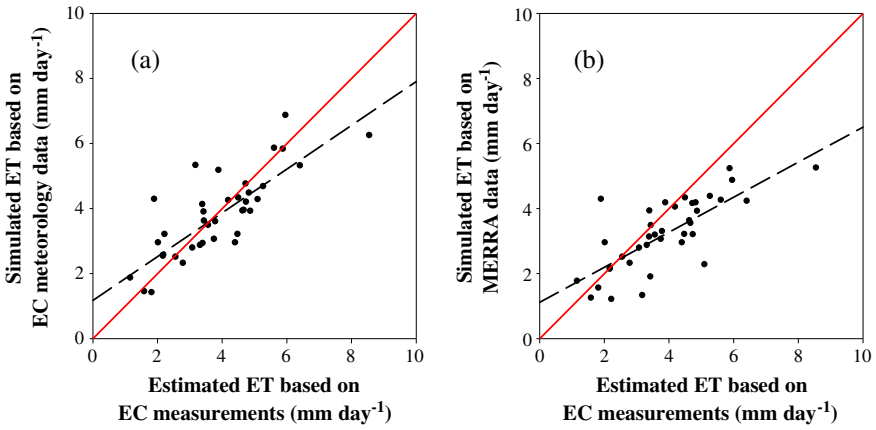

Figure 3. Comparisons of the mean ET observations at each flux tower site and the ET estimates made by the revised RS-PM model. These data were created using (a) tower-specific meteorology ($y = 0{\cdot}67x + 1{\cdot}17$, $R^2 = 0{\cdot}64$) and (b) the regional MERRA meteorology ($y = 0{\cdot}54x + 1{\cdot}12$, $R^2 = 0{\cdot}57$).

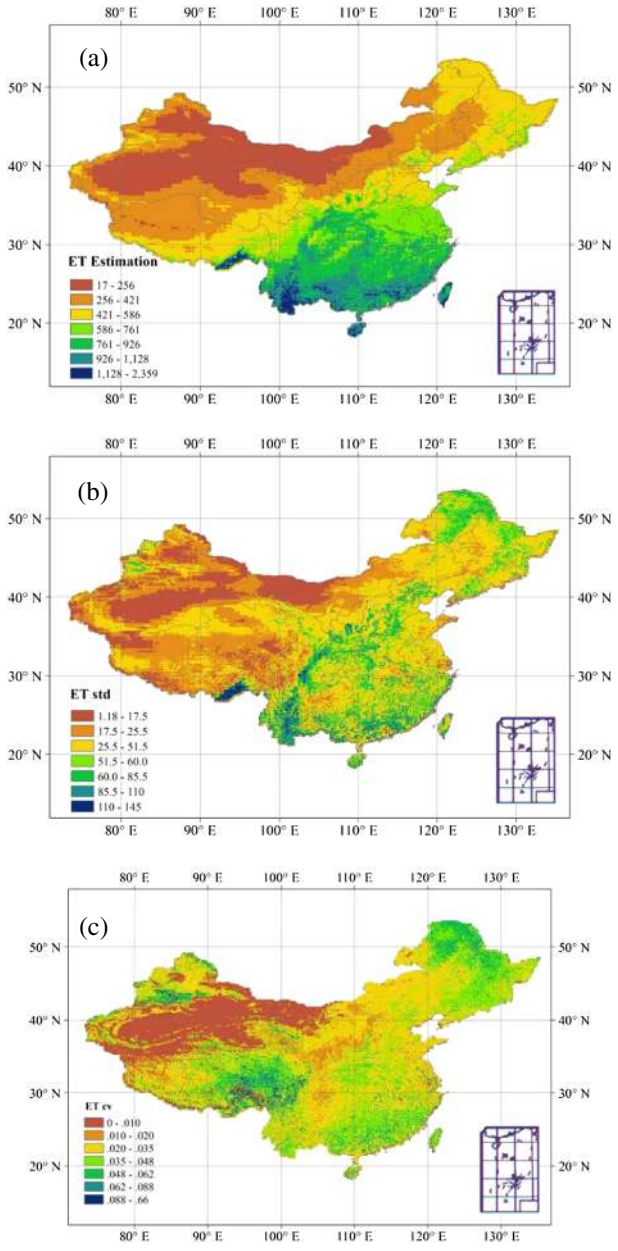

Figure 4. Spatial distribution of the multiyear (1982–2009) mean annual ET estimates as represented by (a) an ET estimation (mm yr^{-1}) driven by interpolated 10 × 10 km MERRA meteorological data averaged from 1982 to 2009, (b) the standard deviation (std, mm yr^{-1}) of modelled ET estimates in a grid cell and (c) the coefficient of variance (CV) of model ET estimated in grid cell. The coefficient of variance is determined by dividing the standard deviation by the mean of the model ET estimates within a grid cell.

estimates ranging from 667 to 854 mm yr^{-1} (Figure 5a). In these locations, both the temperature and moisture requirements were fully satisfied for plantation evaporation. The temperate regions had intermediate ET, and the lowest ET was found in cold arid regions, such as Gansu, Qinghai, Ningxia, Xinjiang and Inner Mongolia, where either the temperature or precipitation was a limiting factor. Although the effect of topography on ET rates is evident through lower ET values in major mountains and in arid/semiarid ranges, the annual ET estimation (345 mm yr^{-1}) of Tibet was comparable with that of northeastern China such as Jilin province. The total ET amount was high in Inner Mongolia, Tibet, Xinjiang and Yunnan, with the values ranging from 261 to 510 km^3 yr^{-1} (Figure 5b).

The spatial distribution of ET was associated with land cover types (Figure 6a). The MODIS land-cover classification product was used to identify 16 different land cover types in China. Relatively high ET densities were found in evergreen broadleaf forest, woody savannas, permanent wetlands and mixed forest, with ET values ranging from 620 to 910 mm yr^{-1}. Although there are some uncertainties, the ET magnitudes and spatial patterns of the estimated ET over different ecosystem types in China are generally consistent with the literatures. Sun *et al.* (2004) investigated that mean annual ET of broadleaf forest is the highest with a value of 566 mm yr^{-1}, whereas the mean annual ET of mixed forests and coniferous forests decreased to 510 and 333 mm yr^{-1}, respectively. In this study, the total ET amount was high in grassland and crop land with a range of 728–771 km^3 yr^{-1} because of the large area of these vegetation types in China (Figure 6b).

Seasonal patterns of ET

The multiyear mean seasonal patterns of ET over the terrestrial ecosystems from 1982 to 2009, using the revised RS-PM algorithm with daily MERRA meteorology and AVHRR LAI inputs, showed seasonal fluctuations (Figure 7). The seasonal patterns of ET and their spatial variability reflected the controlling effects of the climatic conditions. Because of the various climatic zones and the vegetation distributions, the regional ET temporal patterns varied from east to west and from north to south. In the spring (March–May), most parts of South China showed significantly high ET values because the growing season started in early to mid-spring in these regions. Yunnan and Taiwan are dominated by evergreen forests, and these ecosystems also had relatively high ET values because of mild temperatures and moist conditions during the spring. Higher ET values occurred in the Brahmaputra regions in the spring because of a surplus of precipitation, relatively warm temperatures and high radiation. In contrast, low ET was found in the northern regions because of low temperatures. In the summer (June–August), the majority of the northwest region, including the Qinghai-Tibet Plateau and the Inner Mongolian grasslands, continuously exhibited low ET values because of sparse vegetation and precipitation deficits. The northeast regions, which are dominated by temperate broadleaf deciduous forests and warm temperate steppes, showed much higher ET values in the summer than in the spring. In autumn (September–November), the ET values of the southeast regions substantially decreased relative to the ET values in the summer. In the winter (December–February), the majority of the regions of China had little or no photosynthesis because the canopies of most ecosystems were dormant.

Figure 8 shows the trajectories of the spatially averaged ET for different land cover types during the period from 1982 to 2009. Overall, most of the vegetation types had a

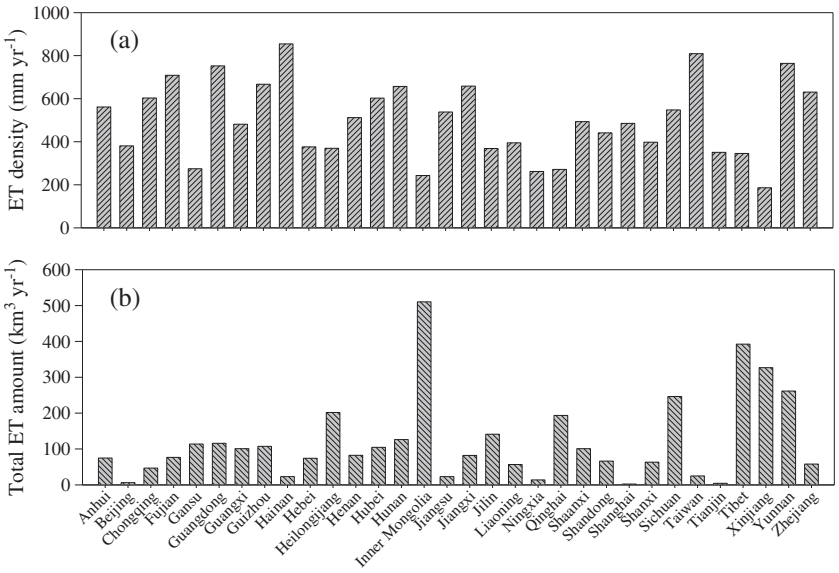

Figure 5. Estimations of average ET density (a) and total amount ET (b) of different provinces in China during the 1982–2009 period.

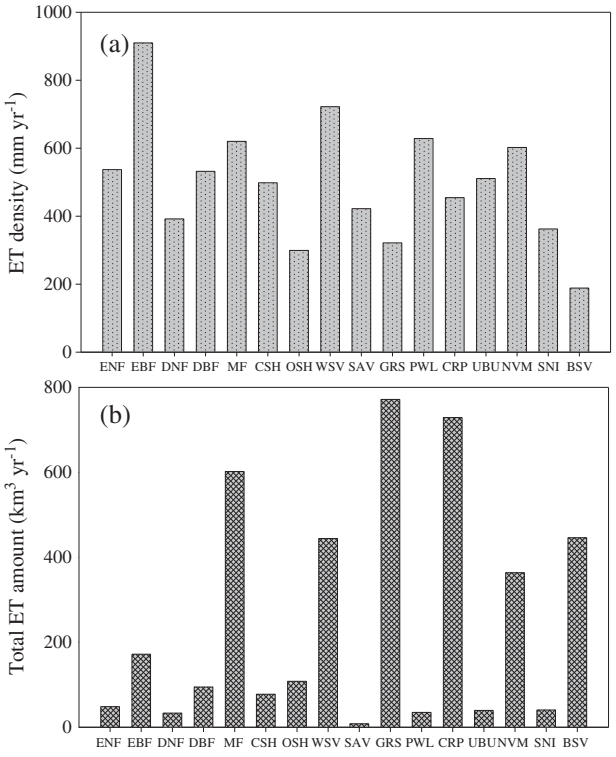

Figure 6. Average ET density (a) and total amount ET (b) over various ecosystems during the 1982–2009 period. Abbreviations: ENF, evergreen needleleaf forest; EBF, evergreen broadleaf forest; DNF, deciduous needleleaf forest; DBF, deciduous broadleaf forest; MF, mixed forest; CSH, closed shrublands; OSH, open shrublands; WSV, woody savannas; SAV, savannas; GRS, grasslands; PWL, permanent wetlands; CRP, croplands; UBU, urban and build up; NVM, natural vegetation mosaic; SNI, snow and ice; BSV, barren or sparsely vegetated.

similar monthly variation, with a maximum in the summer and a minimum in the winter. Deciduous needleleaf forests, deciduous broadleaf forests and savannas had the largest seasonal variation of ET. Closed shrublands, croplands and woody savannas had intermediate intra-annual ET variability. Comparably, evergreen broadleaf forests showed weak seasonality of ET. On average, the monthly ET of various ecosystem types between June and August accounted for 40% of the annual production, whereas the monthly total ET between December and February of the next year contributed only 15% of the annual production in this study.

Interannual variability of ET

China's terrestrial ET varied between 484 and 521 mm yr^{-1} during the1982–2009 period, with a mean value of 500 mm yr^{-1} (Figure 9). In general, the actual ET presented a decreasing trend from 1982 to 2009. Relatively low ET values were found in 1985, 1993, 1997, 2000 and 2009, whereas the highest ET was found in 1998. Recently, the ET values began to decrease during the period from 2003 to 2009 but were still higher than that of 2000. The annual ET in China only accounted for approximately 5·6–8·3% of the world's total land-surface ET when compared with global land-surface ET estimates ranging from 58×10^3 to 85×10^3 km^3 per year during the past 30 years (Dirmeyer *et al*., 2006; Oki and Kanae, 2006; Jung *et al*., 2010). An increasing trend of ET in China was in agreement with Wang *et al*. (2010a, b), who calculated monthly global ET from 1982 to 2002 using a modified PM method and found ET to be increasing by 15 mm yr^{-1}.

Evapotranspiration is the most problematic component of the water cycle to accurately estimate because of the heterogeneity of the landscape and the large number of controlling factors involved, including climate, plant biophysics, soil properties and topography. The absolute interannual variability (indicated as the standard deviation, std) appeared to increase in the mountain ranges at higher elevations, reaching a maximum in the mountains of southwest and northeast China such as Hengduang-Himalayan mountains, the Yunnan-Guizhou plateau, the great Xing'an mountains and the Xiaoxing' an mountains (Figure 4b). The

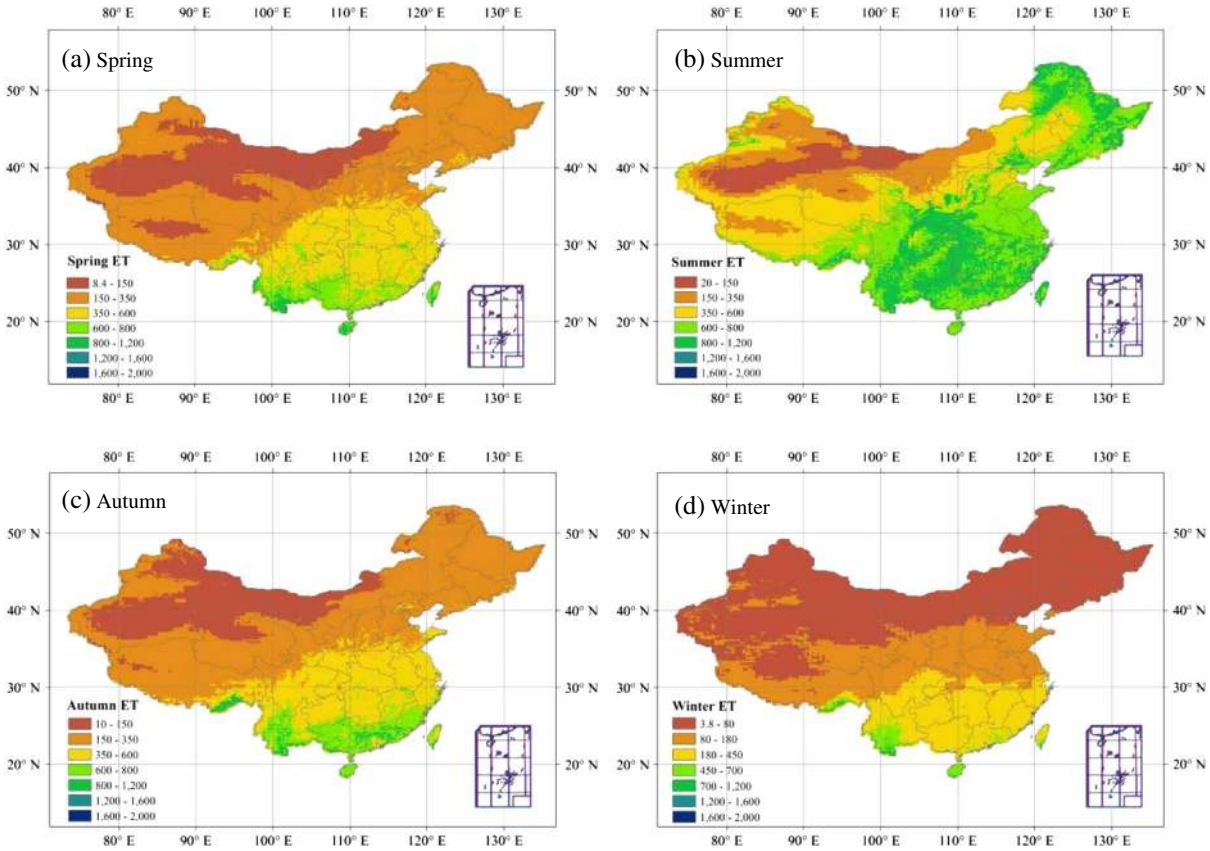

Figure 7. Seasonal distributions of ET (mm season^{-1}) in Chinese terrestrial ecosystems during the 1982–2009 period.

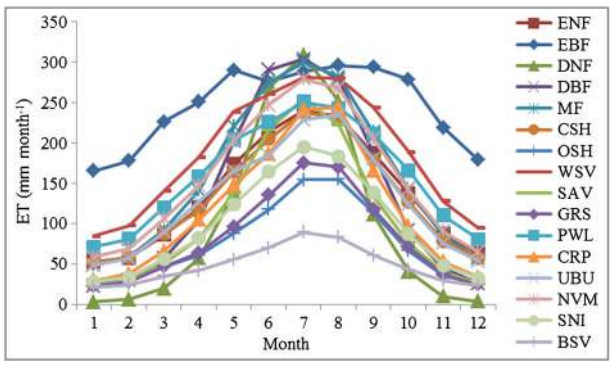

Figure 8. Comparison between the seasonal patterns of ET (mm month^{-1}) under different land use/coverage for evergreen needleleaf forest (ENF), evergreen broadleaf forest (EBF), deciduous needleleaf forest (DNF), deciduous broadleaf forest (DBF), mixed forest (MF), closed shrublands (CSH), open shrublands (OSH), woody savannas (WSV), savannas (SAV), grasslands (GRS), permanent wetlands (PWL), croplands (CRP), Urban and built-up (UBU), natural vegetation mosaic (NVM), snow and ice (SNI) and barren or sparsely vegetated (BSV).

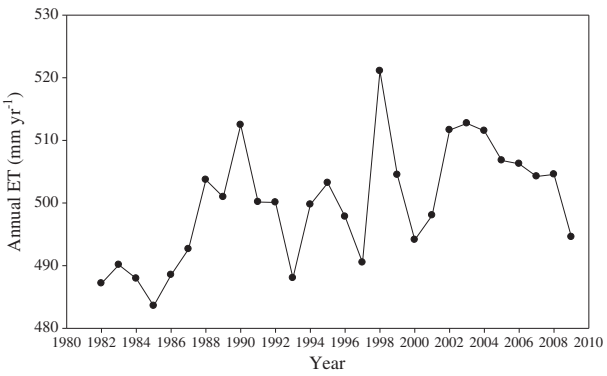

Figure 9. Interannual variations of ET during the 1982–2009 period.

temperate and boreal regions have much higher relative interannual variability than the tropics as shown in CV values (Figure 4c).

Figure 10 shows the coefficient of correlation between environmental factors (i.e. Ta, Rn, and RH) and ET. Generally, for dry conditions, ET contributes to RH, but under moist conditions, Rn drives ET. In detail, Rn has the strongest correlation with ET in humid areas and that the coefficients were less where it is drier, becoming negative in arid areas. Ta and ET are strongly correlated in humid areas but less so far in drier conditions, and their correlation becomes zero or negative in semiarid or arid areas. Wang *et al*. (2010b) also indicated that long-term variations of ET in humid areas are primarily controlled by variations in incident solar radiation; the dominant factor controlling long-term variations of ET in arid areas is soil water supply, estimated here by RH, which is connected to precipitation. In this study, annual RH ($R^2 = 0{\cdot}91$, $p < 0{\cdot}05$), Rn ($R^2 = 0{\cdot}80$, $p < 0{\cdot}05$) and Ta ($R^2 = 0{\cdot}65$, $p < 0{\cdot}05$) are important factors that affected ET variations in overall China's terrestrial ecosystems from 1982 to 2009.

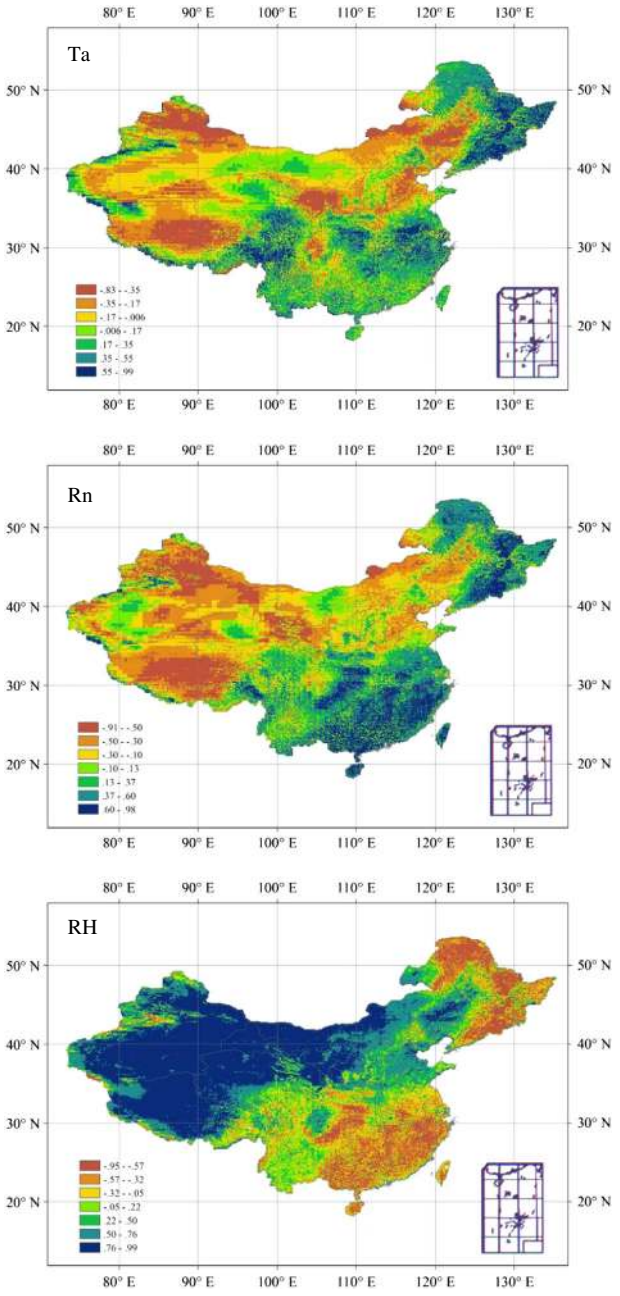

Figure 10. The coefficient of correlation (R) between environmental factors (a) Ta, (b) Rn and (c) RH and ET during the 1982–2009 period.

CONCLUSIONS

On the basis of EC site data and remote sensing data, the revised RS-PM model was successfully used to produce an ET map in China's terrestrial ecosystems. The mean annual land-surface ET was 500 mm yr^{-1} with a range from 484 to 521 mm yr^{-1} in China. Significant seasonal and spatial variations of ET were predicted by the revised RS-PM model. Generally, China's terrestrial ET decreased from southwest China. On average, the annual land-surface ET showed an increasing trend during the period from 1982 to 2009. High ET rates were found in evergreen broadleaf forest, woody savannas, permanent wetlands, and mixed forests. Long-term variations of ET in humid areas such as tropics and humid areas of China are primarily controlled by variations in incident net radiation; however, RH is the dominant factor in controlling long-term variations of ET in arid areas. Although no significant systematic error was found in the revised RS-PM model predictions, the remote sensing-based model explained only 61% of the ET variability across all validation sites. Further study should focus on the development of the RS-PM model from the aspect of stomatal conductance over different ecosystem types.

ACKNOWLEDGEMENTS

We acknowledge the financial support from National Key Basic Research and Development Plan of China (2012CB955501 and 2011CB952001) and the Fundamental Research Funds for the Central Universities. We also acknowledge the US-China Carbon Consortium (USCCC) and some networks such as the Coordinated Observations and Integrated Research over Arid and Semi-arid China (COIRAS) (lead by Key Laboratory of Regional Climate-Environment Research for Temperate East Asia (REC-TEA)), ChinaFlux, AsiaFlux and FluxNet.

REFERENCES

Bastiaanssen WGM, Menenti M, Feddes RA, Holtslag AAM. 1998. A remote sensing surface energy balance algorithm for land (SEBAL): 1. Formulation. *Journal of Hydrology* **212-213**: 198–212.

Baumgartner A, Reichel E. 1975. *The world water balance*. Elsevier: New York.

Chen YH, Li XB, Jing GF, Shi PJ. 2003. An estimation model for daily regional ET. *International Journal of Remote Sensing* **24**(1): 199–205.

Chen D, Gao G, Xu CY, Guo J, Ren GY. 2005. Comparison of the Thornthwaite method and pan data with the standard Penman-Monteith estimates of reference ET in China. *Climate Research* **28**: 123–132.

Chen YH, Li XB, Li J. 2006. A TSAR model for daily ET at broad spatial scales: A case study in Northern China. *Computers & Geosciences* **32**: 476–484.

Cleugh HA, Leuning R, Mu QZ, Running SW. 2007. Regional evaporation estimates from flux tower and MODIS satellite data. *Remote Sensing of Environment* **106**: 285–304.

Cong ZT, Yang DW, Ni GH. 2008. Does evaporation paradox exist in China? *Hydrology and Earth System Sciences* **13**: 357–366.

Dirmeyer PA. 1994. Vegetation stress as a feedback mechanism in mid-latitude drought. *Journal of Climate* **7**: 1463–1483.

Dirmeyer PA, Gao X, Zhao M, Guo ZC, Oki T, Hanasaki N. 2006. GSWP-2: Multimodel Analysis and Implications for Our Perception of the Land Surface. *Bulletin of the American Meteorological Society* **87**: 1381–1397.

Du J, Zhang B, Song KS, Wang ZM, Zeng LH. 2010. Study on ET estimation of Sanjiang Plain based on MODIS product and SEBAL model. *Chinese Journal of Agrometeorology* **31**(1): 104–110. (in Chinese with English abstract)

Fisher JB, Kevin PT, Baldocchi DD. 2008. Global estimates of the landatmosphere water flux based on monthly AVHRR and ISLSCP-II data, validated at 16 FLUXNET sites. *Remote Sensing of Environment* **112**: 901–919.

Gao G, Chen D, Ren GY, Chen Y, Liao YM. 2006. Spatial and temporal variations and controlling factors of potential ET in China: 1956-2000. *Journal of Geophysical Research* **16**(1): 3–12.

Gao G, Chen DL, Xu CY, Simelton E. 2007. Trend of estimated actual ET over China during 1960-2002. *Journal of Geophysical Research* **112**: D11120. doi:10.1029/2006JD008010

Gong L, Xu CY, Chen D, Halldin S. 2006. Sensitivity of the Penman-Monteith reference ET to key climatic variables in the Changjiang (Yangtze River) basin. *Journal of Hydrology* **329**: 620-629. doi:10.1016/j.jhydrol.2006.03.027

Jia L, Xi G, Liu S, Huang C, Yan Y, Liu G. 2009. Regional estimation of daily to annual regional ET with MODIS data in the Yellow River Delta wetland. *Hydrology and Earth System Sciences* **13**: 1775–1787.

Jung M, Reichstein M, Ciais P, Seneviratne SI, Sheffield J, Goulden ML. 2010. Recent decline in the global land ET trend due to limited moisture supply. *Nature* **467**: 951–954. doi:10.1038/nature09396

Kalma JD, Jupp DLB. 1990. Estimating evaporation from pasture using infrared thermometry: Evaluation of a one-layer resistance model. *Agricultural and Forest Meteorology* **51**(3-4): 223–246.

Keane RE, Ryan KC, Veblen TT, Allen CD, Logan J, Hawkes B. 2002. Cascading effects of fire exclusion in Rocky Mountain ecosystems: A literature review. USDA forest service gen. tech. report RMRS-GTR-91 (24 pp.)

Kustas WP, Norman JM. 1996. Use of remote sensing for ET monitoring over land surfaces. *Hydrological Sciences* **41**: 495–516.

Li ZL, Tang RL, Wan ZM, Bi YY, Zhou CH, Tang BH, Yan GJ, Zhang XY. 2009. A review of current methodologies for regional ET estimation from remotely sensed data. *Sensor* **9**: 3801–3853. doi:10.3390/s90503801

Liu BH, Xu M, Mark H, Gong WG. 2004. A spatial analysis of pan evaporation trends in China, 1955 – 2000. *Journal of Geophysical Research* **109**: D15102. doi:10.1029/2004JD004511

McVicar TR, Jupp DLB. 1998. The current and potential operational uses of remote sensing to aid decisions on drought exceptional circumstances in Australia: A review. *Agricultural Systems* **57**: 399–468.

Meyer WS. 1999. Standard reference evaporation calculation for inland, south eastern Australia. Technical Report 35/98, *CSIRO Land & Water*, Adelaide: SA.

Monteith JL. 1964. Evaporation and environment. State and movement of water in living organisms. *Symposia of the Society for Experimental Biology* **19**: 205–234.

Monteith JL. 1965. Evaporation and environment. The state and movement of water in living organisms. Symposium of the society of experimental biology, Vol. 19 (pp. 205-234). Cambridge: Cambridge University Press.

Mu Q, Jones LA, Kimball JS, McDonald KC, Running SW. 2009. Satellite assessment of land surface evapotranspiration for the pan-Arctic domain. *Water Resources Research* **45**: W09420.

Mu QZ, Zhao MS, Heinsch FA, Liu M, Tian H, Running SW. 2007a. Evaluating water stress controls on primary production in biogeochemical and remote sensing based models *Journal of Geophysical Research* **112**: G01012. doi:10.1029/2006JG000179

Mu QZ, Heinsch FA, Zhao MS, Running SW. 2007b. Development of a global Et algorithm based on MODIS and global meteorology data. *Remote Sensing of Environment* **111**: 519–536.

Myneni RB, Keeling CD, Tucker CJ, Asrar G, Nemanl RR. 1997. Increased plant growth in the northern high latitudes from 1981–1991. *Nature* **386**: 698–702.

Oki T, Kanae S. 2006. Global hydrological cycles and world water resources. *Science* **313**: 1068. doi: 10.1126./science.1128845

Penman HL. 1948. Natural evaporation from open water, bare soil and grass. *Proceedings of the Royal Society of London* **A193**: 120–146.

Pielke RS Sr, Avissar R, Raupach M, Dolman AJ, Zeng X, Denning AS. 1998. Interactions between the atmosphere and terrestrial ecosystems: Influence on weather and climate. *Global Change Biology* **4**: 461–475.

Priestley CHB, Taylor RJ. 1972. On the assessment of surface heat fluxes and evaporation using large-scale parameters. *Monthly Weather Review* **100**: 81–92.

Raupach MR. 2001. Combination theory and equilibrium evaporation. *Quarterly Journal of the Royal Meteorological Society* **127**: 1149–1181.

Ruimy A, Kergoat L, Bondeau A. 1999. Comparing global models of terrestrial net primary productivity (NPP): analysis of differences in light absorption and light-use efficiency. *Global Change Biology* **5**: 56–64.

Schreiber L, Skrabs M, Hartmann KD, Diamantopoulos P, Šimáňová E, Šantrůček J. 2001. Effect of humidity on cuticular water permeability of isolated cuticular membranes and leaf disks. *Planta* **214**: 274–282.

Su Z. 2002. The surface energy balance system (SEBS) for estimation of turbulent fluxes. *Hydrology and Earth System Sciences* **6**(1): 85–99.

Sun R, Chen JM, Zhu QJ, Zhou YY, Liu J, Li JT, Liu SH, Yan GJ, Tang SH. 2004. Spatial distribution of ET in Changbaishan Natural Reserve, China, using Landsat ETM + data. *Canadina Journal of Remote Sensing* **30**(5): 731–742.

Sun G, Caldwell P, Noormets A, McNulty SG, Cohen E, Myers JM, Domec JC, Treasure E, Mu QZ, Xiao JF, John R, Chen JQ. 2011. Upscalling key ecosystem functions across the conterminous United States by a water-centric ecosystem model. *Journal of Geophysical Research* **116**: G00J05. doi:10.1029/2010JG001573

Tateishi R. 1996. Mapping ET and water balance for global land surfaces. *Journal of Photogrammetry and Remote Sensing* **51**(4): 209–215.

Thomas A. 2000. Spatial and temporal characteristics of potential ET trends over China. *International Journal of Climatology* **20**: 381–396.

Thomas A. 2008. Development and properties of 0.25-degree gridded ET data fields of China for hydrological studies. *Journal of Hydrology* **358**: 145–158.

Twine TE, Kustas WP, Norman JM, Cook DR, Houser PR, Meyers TP, Prueger JH, Starks PJ, Wesely ML. 2000. Correcting eddy-covariance flux underesti-mates over a grassland, *Agricultural and Forest Meteorology* **103**(3): 279–300.

Vinukollu RK, Wood EF, Ferguson CR, Fisher JB. 2011. Global estimates of ET for climate studies using multi-sensor remote sensing data: Evaluation of three process-based approaches. *Remote Sensing of Environment* **115**: 801–823.

Wang KC, Dickinson RE, Wild M, Liang SL. 2010a. Evidence for decadal variation in global terrestrial ET between 1982 and 2002: 1. Model development. *Journal of Geophysical Research* **115**: D20112, 11 PP. doi:10.1029/2009JD013671

Wang KC, Dickinson RE, Wild M, Liang SL. 2010b. Evidence for decadal variation in global terrestrial ET between 1982 and 2002: 2. Results. *Journal of Geophysical Research* **115**: D20113, 10 PP. doi:10.1029/2010JD013847

Wilson K, Goldstein A, Falge E, Aubinet M, Baldocchi D, Berbigier P, Bernhofer C, Ceulemans R, Dolman H, Field C, Grelle A, Ibrom A. 2002. Energy balance closure at FLUXNET sites. *Agricultural and Forest Meteorology* **113**(1-4): 223–243.

Xiao JF, Chen JQ, Davis KJ, Reichstein M. 2011. Advances in upscaling of eddy covariance measurements of carbon and water fluxes. *Journal of Geophysical Research* **117**: G00J01, doi:10.1029/2011JG001889

Xu CY, Singh VP. 2005. Evaluation of three complementary relationship ET models by water balance approach to estimate actual regional ET in different climatic regions. *Journal of Hydrology* **308**: 105–121. doi:10.1016/j.jhydrol.2004.10.024

Xu CY, Gong LB, Jiang T, Chen D. 2006a. Decreasing reference ET in a warming climate: A case of Changjiang (Yangtze River) catchment during 1970-2000. *Advances in Atmospheric Sciences* **23**: 513–520.

Xu CY, Gong LB, Jiang T, Chen D, Singh VP. 2006b. Analysis of spatial distribution and temporal trend of reference ET in Changjiang catchments. *Journal of Hydrology* **327**: 81–93.

Yuan WP, Liu SG, Zhou GS, Zhou GY, Tieszen LL, Baldocchi D, *et al*. 2007. Deriving a light use efficiency model from eddy covariance flux data for predicting daily gross primary production across biomes. *Agricultural and Forest Meteorology* **143**: 189–207.

Yuan WP, Liu SG, Yu GR, Bonnefond JM, Chen JQ, Davis K, *et al*. 2010. Global estimates of ET and gross primary production based on MODIS and global meteorology data. *Remote Sensing of Environment* **114**: 1416–1431.

Yuan WP, Liu SG, Liang SL, Tan ZX, Liu HP, Young C. 2012. Estimations of evapotranspiration and water balance with uncertainty over the Yukon river basin. *Water Resources Management* **26**: 2147–2157.

Zeng LH, Song KS, Zhang B, Wand ZM, Du J. 2010a. Spatiotemporal variability of reference ET over the Northeast region of China in the last 60 Years. *Advances in Water Science* **21**(2): 194–200.

Zeng LH, Song KS, Zhang B, Wang ZM, Du J. 2010b. Applying SEBAL model and P-M equation to estimate land-surface ET over lower reaches of Wuyu'er River. *Agriculture Research in the Arid Areas* **27**(5): 216–224.

Zhang K, Kimball JS, Hogg EH, Zhao MS, Oechel WC, Cassano JJ, Running SW. 2008. Satellite-based model detection of recent climate-driven changes in northern high-latitude vegetation productivity. *Journal of Geophysical Research* **113**: G03033.

Zhang K, Kimball JS, Nemani RR, Running SW. 2010. A continuous satellite-derived global record of land surface ET from 1983 to 2006. *Water Resources Research* **46**: W09522. doi:10.1029/2009WR008800

Zhao M, Heinsch FA, Nemani R, Running SW. 2005. Improvements of the MODIS terrestrial gross and net primary production global data set. *Remote Sensing of Environment* **95**: 164–176.

